Electron acceleration by laser wakefield and x-ray emission at moderate intensity and density in long plasmas

H. E. Ferrari, A. F. Lifschitz, G. Maynard, and B. Cros

Citation: Phys. Plasmas **18**, 083108 (2011); doi: 10.1063/1.3624771
View online: http://dx.doi.org/10.1063/1.3624771
View Table of Contents: http://pop.aip.org/resource/1/PHPAEN/v18/i8
Published by the American Institute of Physics.

Electron acceleration by laser wakefield and x-ray emission at moderate intensity and density in long plasmas

H. E. Ferrari,[1,2,a)] A. F. Lifschitz,[2] G. Maynard,[2] and B. Cros[2]
[1]*Consejo Nacional de investigaciones científicas y técnicas (CONICET), Bariloche, Argentina*
[2]*Laboratoire de Physique des Gaz et des Plasmas, CNRS-Université Paris Sud 11, Orsay, France*

(Received 27 April 2011; accepted 20 July 2011; published online 22 August 2011)

The dynamics of electron acceleration by laser wakefield and the associated x-rays emission in long plasmas are numerically investigated for parameters close to the threshold of laser self-focusing. The plasma length is set by the use of dielectric capillary tubes that confine the gas and the laser energy. Electrons self-injection and acceleration to the 170 MeVs are obtained for densities as low as 5×10^{18} cm^{-3} and a moderate input intensity (0.77×10^{18} W/cm^2). The associated x-ray emission at the exit of the capillary tube is shown to be an accurate diagnostic of the electrons self-injection and acceleration process. © *2011 American Institute of Physics*. [doi:10.1063/1.3624771]

I. INTRODUCTION

Since the proposition of laser plasma based acceleration,[1] this field is progressing toward a compact alternative to conventional linear accelerators.[2,3] Short pulse duration laser beams, with power above 10 TW, have been shown by numerous groups worldwide to produce accelerated electron bunches, self-injected from the background plasma. Electron beams with energy in the 100 MeVs can be obtained in a few mm long plasmas,[4–6] whereas in 33 mm long plasma channels, electrons in the GeV range have been achieved.[7]

In the laser wakefield mechanism, intense short duration laser pulses interacting with under-dense plasmas expel electrons from the regions of high intensity and leave in their wake a plasma wave. This wave is associated to large amplitude space charge electric fields used to accelerate relativistic electrons. In the non linear regimes of laser wakefield, plasma electrons can be completely blown out of the intense laser region and self-trapped in the accelerating potential of the plasma wave. In addition to the accelerating fields associated to the plasma wave, the accelerated electrons experience transverse fields. Thus, these electrons can undergo strong transverse oscillations, or betatron oscillations, giving rise to the emission of synchrotron like radiation, which has been studied theoretically[8] and observed experimentally.[9–13]

Laser wakefield excitation in long plasmas is of interest for several reasons. In the blown out regime, simulations[14] show that using long plasmas at relatively low density is a way to achieve electron acceleration to the multi-GeV range or beyond. Extending the plasma length is also a way to increase the critical energy of the photons[15] produced through betatron oscillations since it depends mainly on the relativistic factor of accelerated electrons. For a given plasma wave amplitude, electrons will achieve a maximum energy when they are accelerated over the longest possible length in the plasma. Depending on the plasma density and the laser intensity, this length will be determined either by the plasma length, the laser depletion length, or the dephasing length. The dephasing length is the length over which the accelerated electrons will outrun the plasma wave and slip into a decelerating phase. Efforts related to increase the energy of self-injected electrons in the blown out or bubble regimes now rely on decreasing the plasma density, as it results in longer depletion and dephasing lengths, and consequently, on increasing the plasma length.[16,17] However, self-guiding and self-injection will take place for laser power above the critical power for self-focusing.[18,19] At lower intensity, in laser plasma wakefield acceleration schemes where electrons have to be produced by an external source to be injected into the plasma wave, it is desirable to avoid self-injection of background electrons while maintaining the highest possible accelerating field in order to achieve acceleration to high energy. In that case, the extension of the laser propagation in the plasma relies on external guiding, provided by either a plasma channel[20] or a capillary tube for lower densities.[21,22]

It is thus important to determine the threshold for electron self-injection in long plasmas, for parameters relevant to the region intermediate between the blown out regime and the linear regime. The numerical study presented in this paper describes the acceleration of self-injected electrons in long plasmas for parameters close to the threshold of self-focusing. The plasma length is set by the use of dielectric capillary tubes that confine the gas and the laser energy. The results show that in long plasmas, electron self-injection and acceleration can occur at low density and low input intensity, and that the associated x-ray emission is a useful diagnostic for the electrons acceleration process.

The structure of this paper is as follows. In Sec. II, the parameters used and the code are introduced. Section III describes the laser evolution and the electron injection and acceleration inside 20 mm long capillary tubes while the results of x-ray calculations are presented in Sec. IV; conclusions are presented in Sec. V.

II. PARAMETERS AND CODE OVERVIEW

The results of simulations presented in this paper were obtained for parameters close to those of an experiment

a)Electronic mail: ferrarih@cab.cnea.gov.ar.

performed at the Lund Laser Centre.[23] In that experiment, self-injected and accelerated electrons up to 170 MeV, accompanied by x-ray emission, were measured for input intensities as low as 5×10^{17} W/cm^2, for plasma densities down to 5×10^{18} cm^{-3} in 20 mm long capillary tubes, with inner radius between 76 μm and 127 μm filled with hydrogen gas. Plasma densities between 3.5×10^{18} cm^{-3} and 8×10^{18} cm^{-3} were explored.

Three dimensional particle-in-cell (PIC) simulations were performed with the CALDER-CIRC (Ref. 24) code to model electron acceleration and x-ray production in capillary tubes. The capillary tube is modeled by a Heaviside dielectric function, which is 0 inside the capillary and 2.25 in the capillary wall. Part of the simulation domain corresponds to glass (of the order of 25%) where the refracted laser energy is damped. A plasma ramp 400 μm long was used just after the capillary entrance. A peak focused intensity of 0.77×10^{18} W/cm^2 was used in the simulation at the entrance of the capillary tube for all the cases presented in this paper. The simulation was initialized at the capillary entrance using an energy distribution reproducing the azimuthal average of the experimental profile.[25] This profile is airy-like with a first minimum at a radius of 50 μm and 10% of the maximum intensity.

This maximum intensity corresponds to an incident power of 19.3 TW at the entrance of the capillary tube, and a Gaussian pulse duration at full width at half-maximum $\tau = 35$ fs was used. The normalized laser amplitude at the entrance is $a_0 = 0.6$. In the regime $a_0 < 1$, self-injection of electrons is not expected to occur in plasmas a few millimeters long at low density. Simulations were performed for a plasma electron density, n, equal to (3, 5, 6.5, and 8) $\times 10^{18}$ cm^{-3}; the ratio of the pulse length over the plasma wave length, λ_p, was thus changed from 0.56 to 0.9, and both lengths were smaller than the initial spot radius. The ratio between the incident power P to the critical power for self-focusing, $P_{crit} = 17\omega_0^2/\omega_p^2$ GW, changed from 2 to 5.4 for the range of densities explored; ω_0 and ω_p are the incident laser and plasma angular frequencies, respectively. The dephasing length, defined by $L_d = (\omega_0/\omega_p)^2 \lambda_p$, ranges between 10.9 mm for $n = 5 \times 10^{18}$ cm^{-3} and 2.5 mm for the highest density. The laser depletion length, $L_l = (\omega_0/\omega_p)^2 (c\tau)/a_0^2$ calculated for $a_0 = 0.6$ ranges from 10 mm to 6.3 mm for the same densities. Simulations were performed in capillary tubes longer than the dephasing length and the laser depletion length for all values of density.

III. LASER EVOLUTION AND ELECTRON INJECTION

The laser evolution and subsequent electron injection and acceleration are presented in this section for three values of the electron density and a capillary radius of 76 μm.

Figure 1 shows the evolution of the absolute maximum of the normalized laser amplitude a_0, with an initial value $a_0 = 0.6$ at the entrance of the capillary tube, $x = 0$ mm, for electron densities equal to 5 (top graph), 6.5 (middle graph), and 8×10^{18} cm^{-3} (bottom graph). Over the first millimeter of propagation, the evolution of the normalized laser amplitude is not sensitive to the value of the electron density and

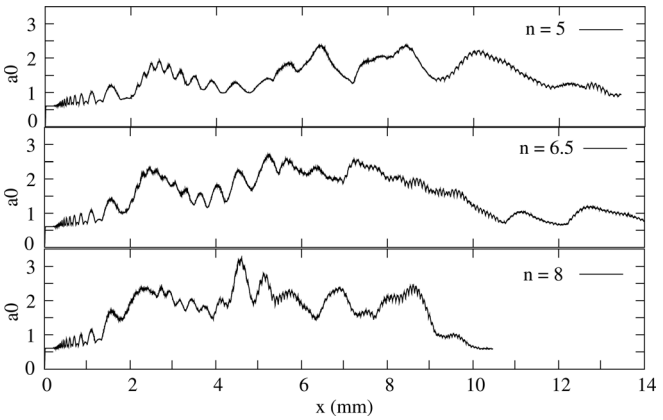

FIG. 1. Evolution of the absolute maximum of the normalized laser amplitude a_0 as a function of the laser position for three different densities, expressed in units of 10^{18} cm^{-3}.

can be attributed to the beating of several modes[26] coupled at the entrance of the capillary. After a distance of 2 mm, under the process of self-focusing, a_0 reaches several maxima with values up to $a_0 \simeq 2.4$ (3.3) for $n = 5(8) \times 10^{18}$ cm^{-3}, respectively. After 10 mm of propagation, the amplitude of a_0 decreases subsequently to the transfer of laser energy to the plasma and losses through the capillary wall.

In Figure 2, the total electron charge for electrons with energy greater than 10 MeV is shown as a function of laser position. It shows that electron injection starts around 2 mm for $n = 6.5$–8×10^{18} cm^{-3} and only after a laser propagation of 6.4 mm, where a_0 reaches the value of 2.4, for $n = 5 \times 10^{18}$ cm^{-3}. No electron injection was observed for the same parameters with a density $n = 3 \times 10^{18}$ cm^{-3}, for which a_0 does not reach this amplitude. For $n = 8 \times 10^{18}$ cm^{-3}, a maximum in the total charge is rapidly achieved and it remains almost constant all along the laser propagation, which is due to beam loading.[27,28] For $n = 6.5 \times 10^{18}$ cm^{-3}, there is a first point of electron injection at 2.2 mm, where a local maximum of a_0 of the order of 2.4 is reached, and a second point of electron injection is located close to 6 mm. For these 3 values of density, electron injection takes place at positions where a_0 reaches the value 2.4. For the same parameters, and $n = 3 \times 10^{18}$ cm^{-3}, $P/P_{crit} \sim 2$ and no injection was observed, whereas injection

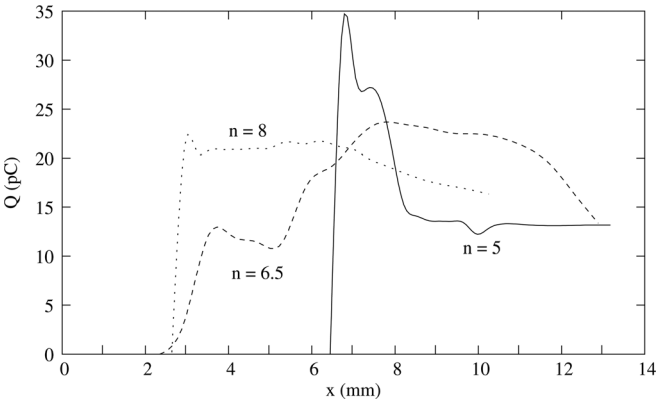

FIG. 2. Accelerated charge Q integrated from 10 to 200 MeV for the same parameters as Figure 1, as a function of laser position. Density expressed in units of 10^{18} cm^{-3}.

occurs for the same incident power and $n = 5 \times 10^{18}$ cm^{-3}, corresponding to $P/P_{crit} \sim 3.3$. These simulation results are in agreement with the value of the threshold for self-injection in low density plasmas which was previously determined from experiment results[18,23] to be $P/P_{crit} \sim 3$.

Figure 3 displays the energy spectra of accelerated electrons as a function of laser position for the three density cases and the same parameters as for Figure 1. These spectra are wide and reflect the fact that the electrons are injected in successive buckets of the plasma wave. For n = 5×10^{18} cm^{-3} [Figure 3(a)], the bunch is accelerated to a maximum energy of 160 MeV at $x = 8.5$ mm and then the energy decreases to a constant value of 90 MeVs. For $n = 6.5 \times 10^{18}$ cm^{-3} [Figure 3(b)], there are three local energy maxima: electrons are injected, accelerated, and decelerated all along the capillary tube, reaching an energy of ~280 MeV at $x = 7.6$ mm, and finally settling in the 200 MeV range. For n = 8×10^{18} cm^{-3} [Figure 3(c)], a maximum energy of 200 MeV is reached at $x = 4.4$ mm while a second peak in the spectrum coexist with a maximum energy of 150 MeV. From these spectra, it can be seen that the position where the maximum energy is reached, and after which the electron energy decreases, is the sum of the injection distance and about half the dephasing length. The fact that the electrons stop gaining energy for a distance shorter than the dephasing length can be attributed to pump depletion, with a length of the order of (10, 7.7, 6.3) mm, for $n = (5, 6.5, 8) \times 10^{18}$ cm^{-3}.

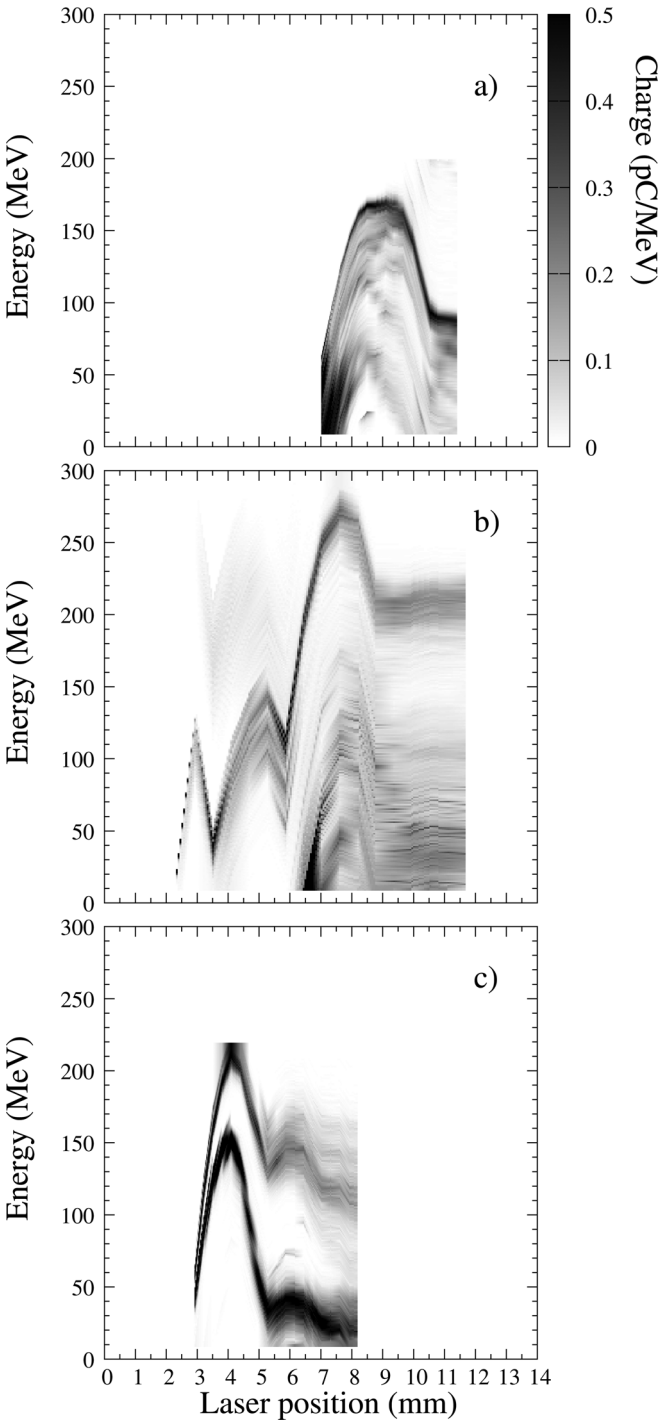

FIG. 3. Energy spectra of accelerated electrons as a function of laser position for electron densities equal to (a) 5, (b) 6.5, and (c) 8×10^{18} cm^{-3}; other parameters are the same as for Figure 1.

The role of the capillary tube can be evaluated by comparing the laser propagation in capillary tubes with different diameters. Figure 4 shows the evolution of the laser amplitude inside two capillary tubes with inner radius 76 μm and 127 μm, and for a density $n = 5 \times 10^{18}$ cm^{-3}. For the wider capillary, the maximum value of the laser amplitude is close to 1.8, whereas for the narrow one, a_0 reaches values close to 2.4. The part of the laser beam initially diffracted and reaching the walls of the capillary tube is reflected back to the axis, contributing to the increase of a_0 on-axis. As the capillary radius increases, this effect becomes smaller because the reflected part of the beam reaches the axis at distances longer than the capillary length. In the case of the wider capillary, the evolution of a_0 is close to the one obtained in a gas jet. Electrons are injected in the narrow capillary around $x = 6.4$ mm, where a_0 is ≈ 2.4. For the same position, the laser amplitude for the wider capillary is $a_0 \simeq 1.8$, and there is no self-injection of electrons. This result is in agreement with experiments,[23] where no electrons were observed for a capillary tube of radius 127 μm, and laser and plasma parameters similar to those of this simulation. Besides the values of a_0, for the narrow capillary, the slope of $a_0(x)$ at the injection point is very steep. This reduces strongly the velocity of the wakefield due to the plasma wavelength enlargement associated with relativistic shift.[29]

Figure 5 shows 100×100 μm^2 maps of normalized electron density (left column) and laser normalized amplitude

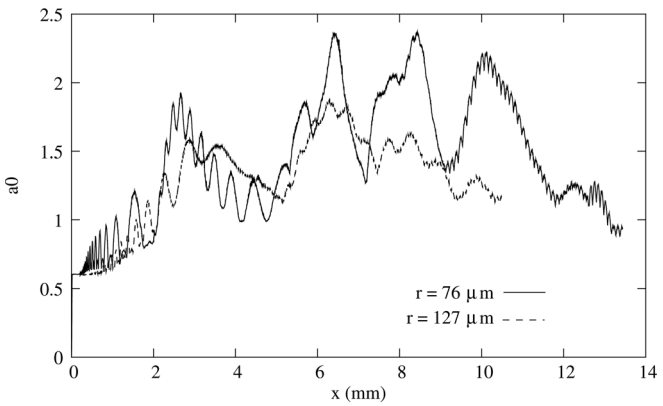

FIG. 4. a_0 evolution for different capillary internal radius, for a density of 5×10^{18} cm^{-3}.

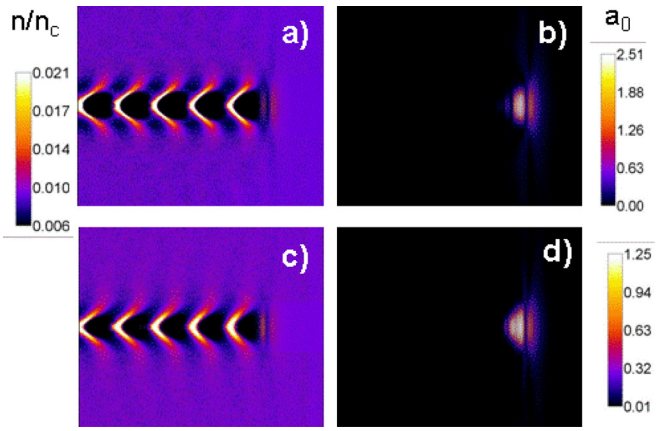

FIG. 5. (Color online) Density normalized to critical density, and normalized laser amplitude in 100×100 μm^2 windows at the position $x = 6.4$ mm for a plasma density 5×10^{18} cm^{-3}, and for 2 values of the capillary inner radius: (a), (b) r = 76 μm, and (c), (d) r = 127 μm.

(right column) at the position $x = 6.4$ mm for two inner capillary radius, $r = 76$ μm [(a) and (b)] and $r = 127$ μm [(c) and (d)]. The laser propagates from left to right and the images are centered vertically on the axis of the capillary tube. As showed above, at this position, electrons are self-injected only for the 76 μm radius case. In this case, the higher laser amplitude leads to higher density values (around 0.1) with a steeper gradient at the back of the cavity. The cavity has a radius of the order of 10 μm. In the case of the larger capillary radius, the laser amplitude peaks at 1.8 and the density at 0.045, the cavity is slightly triangular with a smoother gradient at the back.

IV. X-RAY EMISSION

The x-ray emission is calculated from Lienard-Wiechert potentials,[30] by post-processing the trajectories of electrons with energy larger than 10 MeV obtained in the PIC simulation. The amplitude of the resulting on-axis radiation per unit of frequency and solid angle, $d^2I/d\omega d\theta$, is plotted in Figure 6 as a function of the photon energy for three values of the density and a capillary of radius 76 μm and length 2 cm. Due to the large energy dispersion of the accelerated electrons in the cases of this simulation, the obtained spectra are broader than the on-axis synchrotron like spectra of the type[8] $\xi^2 K_{2/3}^2(\xi)$, obtained for the synchrotron radiation of a mono-energetic beam. Defining phenomenologically, the critical energy, E_c, as the energy for which half the radiated power is in higher energy photons and half is in lower energy photons, it is then possible to characterize the spectra of Figure 6. The integration of the spectra leads to $E_c = (1215, 2765, 2140)$ eV for $n = (5, 6.5, 8) \times 10^{18}$ cm^{-3}, respectively. This critical energy is proportional to the relativistic factor associated to the maximum averaged energy of the first bunch of accelerated electrons, $E_c = 0.0113\gamma_{max}^2$ with a standard deviation of $\pm 4.7 \times 10^{-4}$.

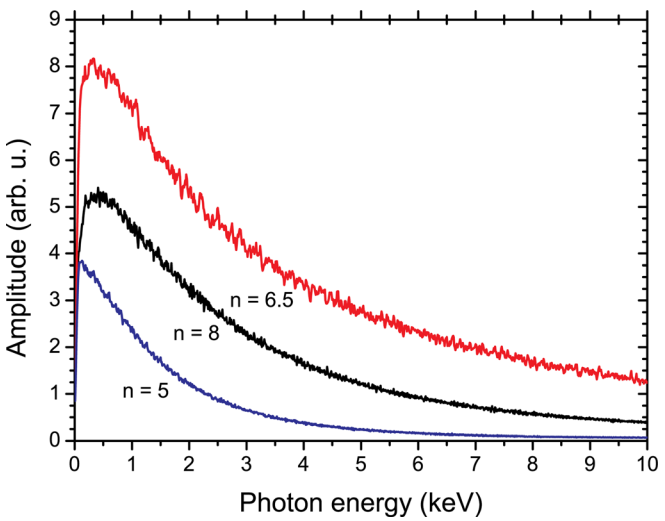

FIG. 6. (Color online) Amplitude of the radiated energy on axis as a function of the photon energy for 3 values of the density in units of 10^{18} cm^{-3}.

The emission cone of the radiation calculated for the electrons populations obtained in these simulations extends up to 50 mrad. From geometrical consideration, it can be seen that the x-rays will reach the capillary wall. The x-rays are assumed to be absorbed at the glass capillary wall. This assumption is valid if the capillary wall surface is not smooth for the considered wavelength range or for large enough incidence angle (measured from the wall surface). As a consequence, only a fraction of the radiation produced along the capillary tube will reach the capillary exit. In order to take this effect into account, we calculate the radiation produced by segments of the trajectories. Due to the finite number of particles, in order to improve the statistics, the emission is calculated over a segment of 1 mm length and averaged over the ensemble of particles in the volume defined by the product of the segment length with the capillary section. For example, to calculate the radiation corresponding to x = 5 mm, we average the radiation of all the particles with trajectories between the positions 4.5 mm and 5.5 mm.

Figures 7–9 exhibit the x-ray amplitude emitted on-axis and integrated from 1 keV to 10 keV, the evolution of the normalized laser amplitude, a_0, and the averaged energy of the first electron bunch, defined as the bunch injected in the first bucket of the plasma wave after the laser pulse, as a function of the laser position for the 3 values of density. The bars used to plot the x-ray emission represent the radiation calculated at each position inside a 1 mm interval. The amplitude of the x-ray emission follows the variation of the

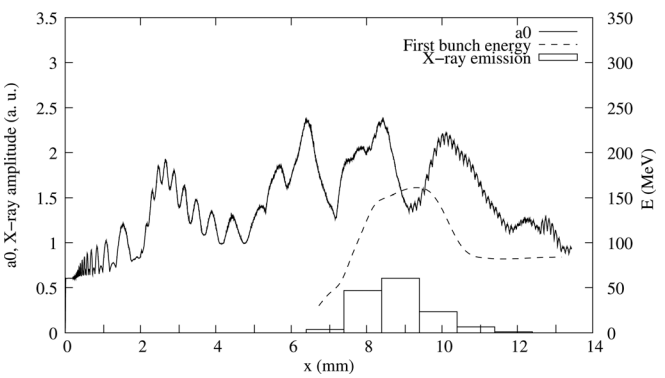

FIG. 7. Normalized laser amplitude, a_0, first bunch averaged energy and x-ray emission as a function of laser position x for $n = 5 \times 10^{18}$ cm^{-3}.

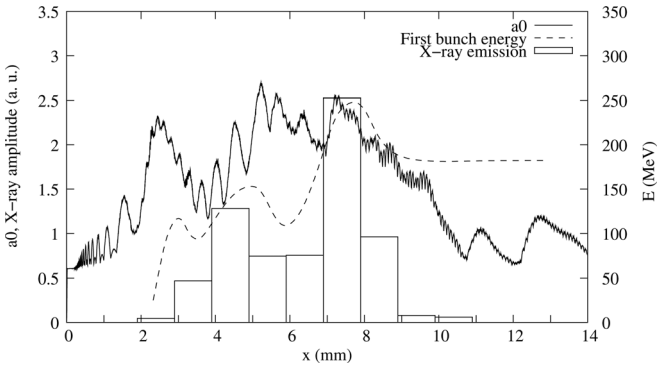

FIG. 8. Same as Figure 7 for $n = 6.5 \times 10^{18}$ cm^{-3}.

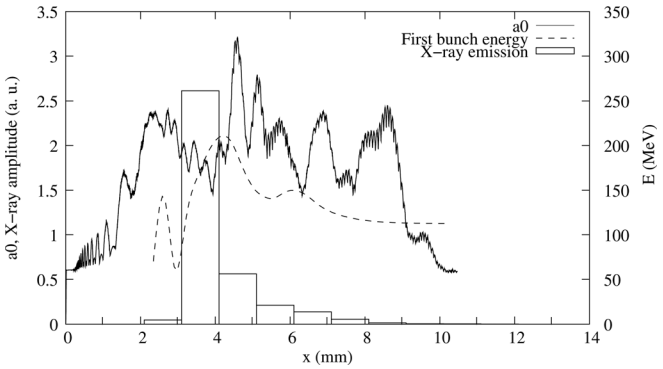

FIG. 9. Same as Figure 7 for $n = 8 \times 10^{18}$ cm^{-3}.

averaged first bunch energy, which is the largest one, reflecting the fact that the emitted power grows[8] as γ^4. The x-ray energy is emitted in the second part of the capillary tube, $x > 6$ mm for $n = 5 \times 10^{18}$ cm^{-3}, at the beginning of the capillary tube, with a peak around 4 mm for $n = 8 \times 10^{18}$ cm^{-3}, and over a larger distance, between 2 and 10 mm for $n = 6.5 \times 10^{18}$ cm^{-3}.

It is of interest, as a diagnostic producing data directly comparable to data accessible experimentally, to calculate the far field emission pattern in a plane perpendicular to the capillary tube, at a position situated after the exit of the tube. In Figure 10, the far field emission calculated at the exit of a 2 cm long capillary tube is shown for the 3 different densities. Figure 10 shows that the beam size and energy distribution are functions of the electron density, which confirms previous experimental observations.[23] More specifically, together with Figures 7–9, it shows that the beam diameter is larger when the source of x-ray emission is closer to the exit of the tube, and that the change of intensity along the beam radius is related to the existence of an extended source ($n = 6.5 \times 10^{18}$ cm^{-3} case). The resulting x-ray beam diameter is thus a combination of the position and extension of the x-ray source, determined by the electron injection and acceleration process, and of the geometrical aperture determined by the capillary tube diameter and length. It is thus possible to use the characterization of the x-ray beam energy distribution in the far field plane to infer the position of the x-ray source inside the tube. The energy distribution obtained from simulations with a dynamic range of 10^{-13} was averaged over the angle and plotted as a function of the radius in logarithmic scale in order to determine the extension of the beam. For example, for the case $n = 5 \times 10^{18}$ cm^{-3}, the divergence of the x ray far field measured from the x-ray profile obtained from the image of Fig. 10 is ± 6.04 mrad and the edge of the beam extends to ± 9.39 mrad. For the capillary radius of 76 μm and 2 cm length, the position of the start of the x-ray emission is calculated as $x_s = 20 - 76/6.04 = 7.4$ mm and it ends at $x_e = 20 - 76/9.39 = 11.9$ mm. It can be checked in Figure 7 that this measurement of the x-ray beam radius gives an accurate determination of the x-ray source position and extension along the laser axis.

With the parameters used in this simulation, Figures 7–9 also show that the peak emission of the x-ray occurs when the first bunch reaches its maximum energy. In Figure 11, the position of the peak electron energy is plotted as a function of the electron density, together with the average position of the x-ray emission calculated from the average x-ray beam radius in the far field plane. For the electron peak, energy position error bars arise from the window measurement time (0.6 mm). The agreement between these two determinations of the peak energy position shows that the measurement of the x-ray beam energy distribution can be

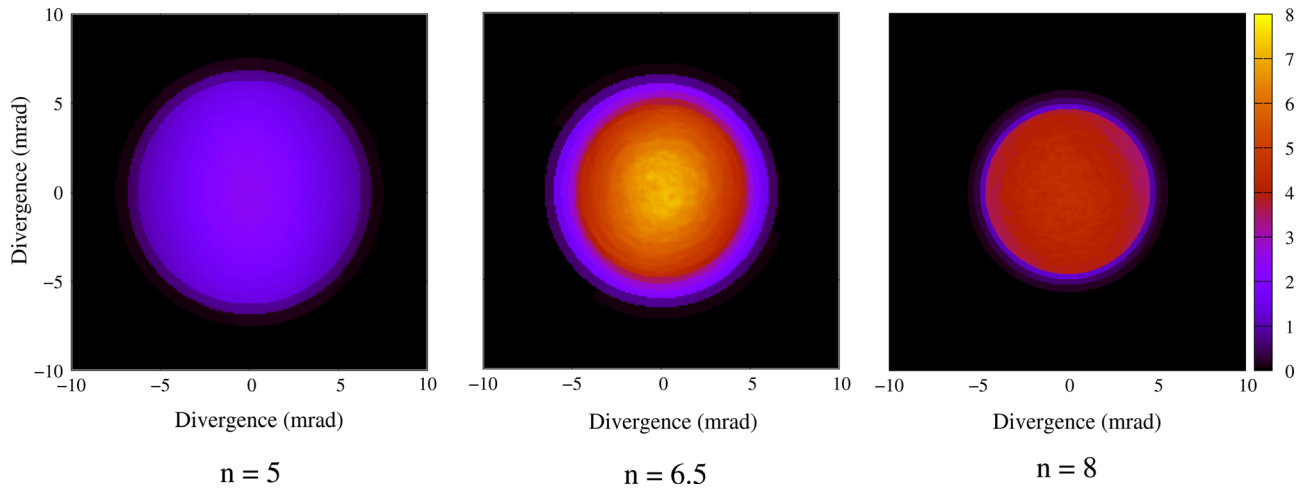

FIG. 10. (Color online) Far field x-ray emission pattern calculated in the transverse plane at the exit of a 2 cm long capillary tube of radius 76 μm for the different densities.

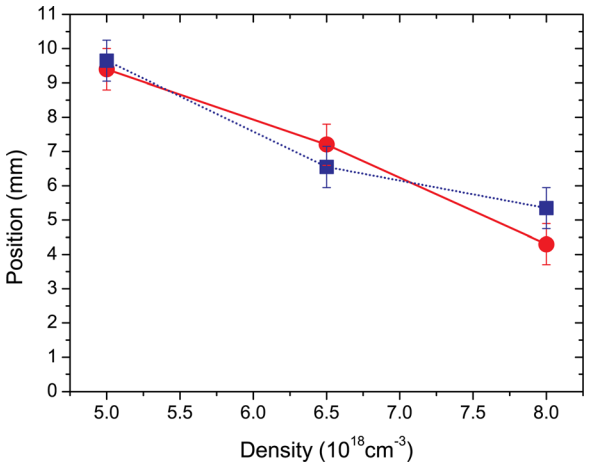

FIG. 11. (Color online) Position of the peak electron energy calculated from x-ray beam radius (blue square) and from electron spectra (red dots) as a function of plasma density.

an accurate diagnostic of the acceleration process in this parameter range.

V. CONCLUSION

We have presented a numerical analysis of electron self-injection and acceleration and of the associated x-ray emission in capillary tubes, allowing to create long plasmas at moderate densities. At moderate intensity and density, the confinement of laser energy by the capillary tube contributes to increase the initial intensity up to the threshold for electrons self-injection, which is not achieved by self-focusing alone. Starting with an initial value of the laser normalized amplitude lower than 1, a long enough distance of propagation, with the help of external guiding, can thus lead to self-injection of background electrons, which was found to occur when the value of the laser normalized amplitude reaches 2.4 for the three values of density examined here. While in free space the phase velocity of the plasma wave decreases for higher plasma density and can help self-injection at lower plasma wave, and laser amplitude, the propagation inside a capillary tube can be more complex due to the excitation and beating of several modes. For the input laser profile considered here inside a capillary, the group velocity of the laser depends on the density and also on the modes excited at the entrance of the tube. In particular, the beating of several modes can lead locally to a higher laser amplitude for a lower group velocity compared to single mode propagation. For example in the case $n=6.5\times10^{18}$ cm^{-3}, there is a small bunch injected close to $x=2$ mm, which does not occur when the simulation is initialized with a Gaussian profile. With a Gaussian profile, the fast oscillation of a_0 disappears and no bunch will be injected for $n=6.5\times10^{18}$ cm^{-3} until $x=5$ mm. The plasma density plays a role on the amount of injected charge and the distance over which injection occurs as can be seen in Fig. 2, by comparing the $n=6.5\times10^{18}$ cm^{-3} and $n=8\times10^{18}$ cm^{-3} cases.

The accelerated electrons spectra were calculated and it was shown that the x-ray emission can be used as a diagnostic to determine the region of the plasma where the x-ray is produced and where the maximum electron energy is achieved. The critical energy associated to the x-ray emission is found to be proportional to the maximum relativistic factor associated to the maximum averaged electron energy, even if the x-ray spectra are broader than the synchrotron like spectra. The x-ray beam diameter measured after the exit of the capillary tube is found to change with the longitudinal position and extension of the x-ray source, which depends on the plasma density, in agreement with experimental results.[23]

ACKNOWLEDGMENTS

H.E. Ferrari acknowledges financial support by CONICET (Argentina) and by the RTRA Triangle de la Physique Contract No. 2007-28 APPEAL.

[1]T. Tajima and J. Dawson, Phys. Rev. Lett. **43**, 267 (1979).
[2]E. Esarey, P. Sprangle, and A. Ting, IEEE Trans. Plasma Sci. **24**, 252 (1996).
[3]C. Joshi and T. Katsouleas, Phys. Today **56**(6), 47 (2003).
[4]S. P. D. Mangles, C. D. Murphy, Z. Najmudin, A. G. R. Thomas, J. L. Collier, A. E. Dangor, E. J. Divall, P. S. Foster, J. G. Gallacher, C. J. Hooker, D. A. Jaroszynski, A. J. Langley, W. B. Mori, P. A. Norreys, F. S. Tsung, R. Viskup, B. R. Walton, and K. Krushelnick, Nature **431**, 535 (2004).
[5]C. G. R. Geddes, Cs. Toth, J. van Tilborg, E. Esarey, C. B. Schroeder, D. Bruhwiler, C. Nieter, J. Cary, and W. P. Leemans, Nature **431**, 538 (2004).
[6]J. Faure, Y. Glinec, A. Pukhov, S. Kiselev, S. Gordienko, E. Lefebvre, J.-P. Rousseau, F. Burgy, and V. Malka, Nature **431**, 541 (2004).
[7]W. P. Leemans, B. Nagler, A. J. Gonsalves, Cs. Tóth, K. Nakamura, C. G. R. Geddes, E. Esarey, C. B. Schroeder, and S. M. Hooker, Nat. Phys. **2**, 696 (2006).
[8]E. Esarey, B. A. Shadwick, P. Catravas, and W. P. Leemans, Phys. Rev. E **65**, 056505 (2002).
[9]M. Schmitz and H. J. Kull, Europhys. Lett. **58**, 382 (2002).
[10]S. Kiselev, A. Pukhov, and I. Kostyukov, Phys. Rev. Lett. **93**, 135004 (2004).
[11]A. Rousse, K. T. Phuoc, R. Shah, A. Pukhov, E. Lefebvre, V. Malka, S. Kiselev, F. Burgy, J.-P. Rousseau, D. Umstadter, and D. Hulin, Phys. Rev. Lett. **93**, 066403 (2004).
[12]S. Kneip, S. R. Nagel, C. Bellei, N. Bourgeois, A. E. Dangor, A. Gopal, R. Heathcote, S. P. D. Mangles, J. R. Marquès, A. Maksimchuk, P. M. Nilson, K. Ta Phuoc, S. Reed, M. Tzoufras, F. S. Tsung, L. Willingale, W. B. Mori, A. Rousse, K. Krushelnick, and Z. Najmudin, Phys. Rev. Lett. **100**, 105006 (2008).
[13]D. B. Thorn, C. G. R. Geddes, N. H. Matlis, G. R. Plateau, E. H. Esarey, M. Battaglia, C. B. Schroeder, S. Shiraishi, Th. Stöhlker, C. Tóth, and W. P. Leemans, Rev. Sci. Instrum. **81**, 10E325 (2010).
[14]W. Lu, M. Tzoufras, C. Joshi, F. S. Tsung, W. B. Mori, J. Viera, R. A. Fonseca, and L. O. Silva, Phys. Rev. ST Accel. Beams **10**, 061301 (2007).
[15]S. Kneip, C. mcGuffey, J. L. Martins, S. F. Martins, C. Bellei, V. Chvykov, F. Dollar, R. Fonseca, C. Huntington, G. Kalintchenko, A. Maksimchuk, S. P. D. Mangles, T. Matsuoka, S. R. Nagel, C. A. J. Palmer, J. Schreiber, K. ta Phuoc, A. G. R. Thomas, V. Yanovsky, L. O. Silva, K. Krushelnick, and Z. Najmudin, Nat. Phys. **6**, 980 (2010).
[16]J. E. Ralph, K. A. Marsh, A. E. Pak, W. Lu, C. E. Clayton, F. Fang, W. B. Mori, and C. Joshi, Phys. Rev. Lett. **102**, 175003 (2009).
[17]J. E. Ralph, C. E. Clayton, F. Albert, B. B. Pollock, S. F. Martins, A. E. Pak, K. A. Marsh, J. L. Shaw, A. Till, J. P. Palastro, W. Lu, S. H. Glenzer, L. O. Silva, W. B. Mori, C. Joshi, and D. H. Froula, Phys. Plasmas **17**, 056709 (2010).
[18]D. H. Froula, C. E. Clayton, T. Dppner, K. A. Marsh, C. P. J. Barty, L. Divol, R. A. Fonseca, S. H. Glenzer, C. Joshi, W. Lu, S. F. Martins, P. Michel, W. B. Mori, J. P. Palastro, B. B. Pollock, A. Pak, J. E. Ralph, J. S. Ross, C. W. Siders, L. O. Silva, and T. Wang, Phys. Rev. Lett. **103**, 215006 (2009).
[19]J. Osterhoff, A. Popp, Zs. Major, B. Marx, T. P. Rowlands-Rees, M. Fuchs, M. Geissler, R. Hrlein, B. Hidding, S. Becker, E. A. Peralta, U. Schramm, F. Grner1, D. Habs, F. Krausz, S. M. Hooker, and S. Karsch, Phys. Rev. Lett. **101**, 085002 (2008).

[20]D. J. Spence and S. M. Hooker, Phys. Rev. E **63**, 015401 (2000).
[21]F. Wojda, K. Cassou, G. Genoud, M. Burza, Y. Glinec, O. Lundh, A. Persson, G. Vieux, E. Brunetti, R. P. Shanks, D. Jaroszynski, N. E. Andreev, C.-G. Wahlstrm, and B. Cros, Phys. Rev. E **80**, 066403 (2009).
[22]N. E. Andreev, K. Cassou, F. Wojda, G. Genoud, M. Burza, O. Lundh, A. Persson, B. Cros, V. E. Fortov, and C.-G. Wahlstrom, New J. Phys. **12**, 045024 (2010).
[23]G. Genoud, K. Cassou, F. Wojda, H. E. Ferrari, C. Kamperidis, M. Burza, A. Persson, J. Uhlig, S. Kneip, S. P. D. Mangles, A. Lifschitz, B. Cros, and C.-G. Wahlstrom, Appl. Phys. B online publication.
[24]A. F. Lifschitz, X. Davoine, E. Lefebvre, J. Faure, C. Rechatin, and V. Malka, J. Comput. Phys. **228**, 1803 (2009).
[25]H. E. Ferrari, A. Lifschitz, and B. Cros, Plasma Phys. Controlled Fusion **53**, 014005 (2011).
[26]B. Cros, C. Courtois, G. Matthieussent, A. Di Bernardo, D. Batani, N. Andreev, and S. Kuznetsov, Phys. Rev. E **65**, 026405 (2002).
[27]M. Tzoufras, W. Lu, F. S. Tsung, C. Huang, W. B. Mori, T. Katsouleas, J. Vieira, R. A. Fonseca, and L. O. Silva, Phys. Rev. Lett. **101**, 145002 (2008).
[28]C. Rechatin, X. Davoine, A. Lifschitz, A. Ben Ismail, J. Lim, E. Lefebvre, J. Faure, and V. Malka, Phys. Rev. Lett. **103**, 194804 (2009).
[29]A. Oguchi, A. Zhidkov, K. Takano, E. Hotta, K. Nemoto, and K. Nakajima, Phys. Plasmas **15**, 043102 (2008).
[30]J. D. Jackson, *Classical Electrodynamics*, 2nd ed. (John Wiley & Sons, New York, 1975).